

Available online at website: https://journal.bcrec.id/index.php/bcrec

Bulletin of Chemical Reaction Engineering & Catalysis, 20 (1) 2025, 44-52



Research Article

Photocatalytic Mechanism and Charge Transfer of PtS₂/WSe₂ Heterostructures: First-principles Study

Zhaonan Sun¹, Yuxuan Song², Wendi Lv², Xiangyu Zeng², Zhongtian Fu*^{2,3}

¹Liaoning Provincial Key Laboratory of Energy Storage and Utilization, Yingkou Institute of Technology, Yingkou 115014, P.R. China.

²School of Resources and Civil Engineering, Northeastern University, Shenyang, Liaoning, 110819, P.R. China. ³Key Laboratory of Ministry of Education on Safe Mining of Deep Metal Mines, Northeastern University, Shenyang, Liaoning, 110819, P.R. China.

Received: 8th November 2024; Revised: 4th January 2025; Accepted: 5th January 2025 Available online: 7th January 2025; Published regularly: April 2025



Abstract

To address the recombination problem of photogenerated electrons and holes during photocatalysis, strategies to design composite photocatalysts with heterojunction structures have been widely adopted. In order to explore the electron transfer pathway and photocatalytic mechanism of the PtS_2/WSe_2 heterostructure, the band structure, electronic properties and catalytic activity of the structure were systematically calculated by density functional theory (DFT). We designed two models consisting of PtS_2 and WSe_2 monolayers to find more stable structures through adsorption energy calculations. In this work, Mulliken charge analysis and differential charge density confirmed the heterojunction as an S-scheme heterojunction. Due to the height difference between the Fermi levels of the two pristine semiconductors, electrons flow from WSe_2 to PtS_2 to form a built-in electric field and band bending. The properties of the S-scheme heterojunction allow the heterostructure to possess a suitable band gap without losing the redox ability, thereby ensuring that the PtS_2/WSe_2 heterostructure can spontaneously undergo HER and OER processes of water splitting.

Copyright © 2025 by Authors, Published by BCREC Publishing Group. This is an open access article under the CC BY-SA License (https://creativecommons.org/licenses/by-sa/4.0).

Keywords: DFT; heterostructure; S-scheme; band gap water splitting

How to Cite: Sun, Z., Song, Y., Lv, W., Zeng, X., Fu, Z. (2025). Photocatalytic Mechanism and Charge Transfer of PtS₂/WSe₂ Heterostructures: First-principles Study. Bulletin of Chemical Reaction Engineering & Catalysis, 20 (1), 44-52. (doi: 10.9767/bcrec.20249)

Permalink/DOI: https://doi.org/10.9767/bcrec.20249

1. Introduction

The problem of energy shortage has attracted more and more attention all over the world [1-4]. In recent years, people have been working to obtain hydrogen by splitting water through photocatalytic technology [5-10]. Therefore, the search for photocatalysts with strong redox ability and low cost has become a research hotspot. The strategy of using a single photocatalyst as a substrate to dope atoms was adopted to improve the band structure and catalytic activity by some researchers. However, these mutually doped impurity regions are easy to become the

recombination centers of new photo-generated charges, resulting in reducing mobility and water splitting efficiency [11]. Notably, van der Waals (vdWs) heterostructures with Type-II [12-13] band alignment have been proposed, but there are still contradictions unresolved. The smaller band gap makes the absorption and excitation of photons easier, however, the energy level potentials of the conduction and valence bands should contain the redox potential of the catalytic reaction, which widens the band gap and weakens the absorption of solar photons. In 2019, Yu et al. first proposed an S-type photocatalyst. The WO₃ and g-C₃N₄ nanosheets were used to construct a heterojunction system to study the charge transfer path during the process of photo-splitting

* Corresponding Author.

Email: fuzhongtian@mail.neu.edu.cn (Z. Fu)

water for hydrogen production [14]. This principle can explain the law between light absorption range and redox ability in heterojunction structures, so it has attracted many researchers' attention [15-19].

Transition metal dichalcogenides (TMDs) [20-21] are widely used in the field of catalysis because of their layered structure similar to graphene [22], strong in-plane covalent bonds in the layer, high performance, low energy consumption and low cost. Most single-layer TMD has a direct band gap, and with the increase of the number of layers, the direct band gap may change into an indirect band gap [23-24].

Currently, photocatalytic water splitting research focuses on Group-6 TMDs, such as MoS₂, while less research on Group-10 TMDs (PtS₂ and PtSe₂). Notably, PtS₂ and PtSe₂ are considered ideal photocatalysts for water splitting due to their suitable band-edge positions and their excellent properties, such as strong interlayer interactions and high carrier mobility [25].

In this work, PtS₂ and WSe₂ in TMDs were used to construct heterostructures to discuss the law of electronic structure and photogenerated carrier transfer of PtS₂/WSe₂ heterostructures. Electron density difference and Mulliken charge analysis convincingly demonstrate that the PtS₂/WSe₂ heterostructure belongs to the Sscheme. The recombination of photogenerated electron-hole pairs with weak redox ability will be enhanced and the separation rate of carriers with strong redox ability will beimproved by the formation of the built-in electric field and band bending effectively. Therefore, the water splitting of PtS₂/WSe₂ heterostructures may spontaneously proceed.

2. Methods

The effect of the interaction among valence electrons and ionic nuclei is characterized by the ultrasoft pseudopotential. Electronic structure computations employed an energy cutoff of 450 eV and utilized Monkhorst-Pack [26] k-point meshes

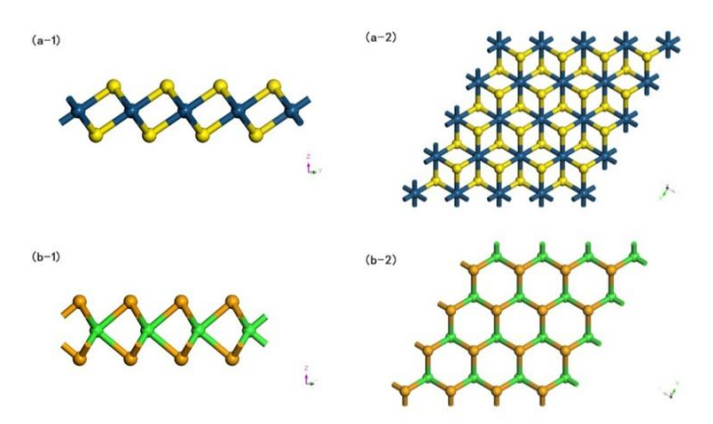


Figure 1. Side and top views of the PtS₂ monolayer (a) and WS₂ monolayer (b)

with a grid density of 3×3×1. During the geometric optimization process, the atomic positions within the model were adjusted iteratively towards the minima of the potential energy surface until the convergence criteria for energy, maximum force, and maximum displacement were met, with thresholds set at 1.0×10-5 eV per atom, 0.03 eV/Å, and 0.001 Å, respectively. A description of van der Waals interactions with long-range electronic effects implemented the Tkatchenko and Scheffler (TS) correction [25].

The electronic and optical properties of the heterojunction catalysts were investigated using the CASTEP, with the exchange-correlation energies treated using the Perdew-Burke-Ernzerhof (PBE) functional [28]. To address the strong electron correlations accurately, the DFT/GGA + U method was invoked, incorporating an on-site Coulombic correction to overcome the band gap underestimation associated with the GGA approximation. In this study, the Hubbard U parameters for molybdenum (UMo) and tungsten (UW) were set at 3.5 eV and 4.0 eV, respectively.

3. Results and Discussion

The geometrical structures of 2H-phase bulk PtS2 and WSe2 were relaxed first, the bilayer models were built by cleaving bulk PtS₂ and WSe₂ along the (001) direction. The lattice parameters of PtS2 and WSe2 after geometric optimization are 3.19032 Å and 3.19073 Å, respectively, it is consistent with the existing experimental and theoretical research results [29-30]. constructed model calculated in this work is a 4×4×1 supercell that contains 16 Mo atoms, 16 W atoms and 64 S atoms with 15 Å vacuum added in the z direction to avoid the interactions between neighbor slabs (see Figure 1). The PtS2/WSe2 heterostructure bilayers are extremely matched, and the average lattice mismatch is less than 1%, which can reflect the heterostructure more realistically. Table 1 shows the structural parameters and bond lengths after geometric optimization of all the models in this work.

3.1 Adsorption Energy Calculation

In this paper, two binding modes of PtS_2 and WSe_2 are discussed, and the most stable structure will be selected for subsequent analysis by calculating the adsorption energy. The heterojunction models constructed based on these two different combinations were shown in Figure $^{\circ}$

The following equation shows the calculate method of the energy of adsorption (EADS):

$$E_f = E_{PtS_2/WSe_2} - E_{WSe_2} - E_{PtS_2} \tag{1}$$

where $E_{PtS2/WSe2}$, E_{WSe2} and E_{PtS2} represent the total energy of the heterojunction structure, monolayer WSe_2 and monolayer PtS_2 , respectively, which were calculated by building a single layer of pristine semiconductors. Based on this definition, a more negative adsorption energy implies stronger adsorption. The calculated adsorption energies are listed in Table 2. The adsorption energy of Model A is negative, indicating that its existence is stable. We speculate that the system tends to be unstable

Table 2. The adsorption energy of Model A and Model B

Model A	Model B
-1.1345eV	$0.1374 \mathrm{eV}$

because of the Coulomb repulsion when the Se atoms and S atoms face each other in the Model B interface region.

3.2 Band Structure and Density of States Analysis

For catalysts, the energy band structure and the corresponding density of states are one of the important means to analyze their performance [31]. In this paper, the energy band structures of the two models are firstly calculated and compared with bulk PtS_2 and bulk WSe_2 . The results are shown in Figure 3.

Both the single semiconductor Model and the two heterostructure models exhibit indirect band gaps. The band gaps ($E_{\rm g}$) of PtS₂ and WSe₂ are 1.593 eV and 1.505 eV, respectively, which are consistent with the experimental results,

Table 1. Structure parameters, bond lengths (Å) and bond populations of PtS2, WSe2, and PtS2/WSe2.

	Structure Parameters			Dand	Bond	Bond
	a/Å	b/Å	c/Å	Bond	Length/Å	Population
PtS_2	14.32028	14.32028	3.25087	S_1 -Pt	2.40444	0.45
F 1.52	14.52026	14.52026		S_2 -Pt	2.40444	0.45
WSe_2	13.30828	13.30828	15.0690	Se_1 - W_1	2.55271	0.53
WSe_2 13.3	15.50626	15.50626	15.0690	$\mathrm{Se}_2 ext{-}\mathrm{W}_1$	2.55271	0.53
				S_2 -Pt ₁	2.37013	0.53
PtS ₂ /WSe ₂ (Model A) 12.61160	10.01100	05 0040	S_1 -Pt ₁	2.37327	0.37	
	12.61160	0 12.61160	25.3948	$\mathrm{Se}_{2} ext{-}\mathrm{W}_{1}$	2.54967	0.75
				$\mathrm{Se}_{1} ext{-}\mathrm{W}_{1}$	2.56560	1.17
				S_2 -Pt ₁	2.37012	0.49
PtS ₂ /WSe ₂ (Model B)	13.63880	13.63880	27.2114	S_1 -Pt ₁	2.37326	0.34
				$\mathrm{Se}_{2} ext{-}\mathrm{W}_{1}$	2.54974	0.77
				$\mathrm{Se}_{1} ext{-}\mathrm{W}_{1}$	2.56554	1.16

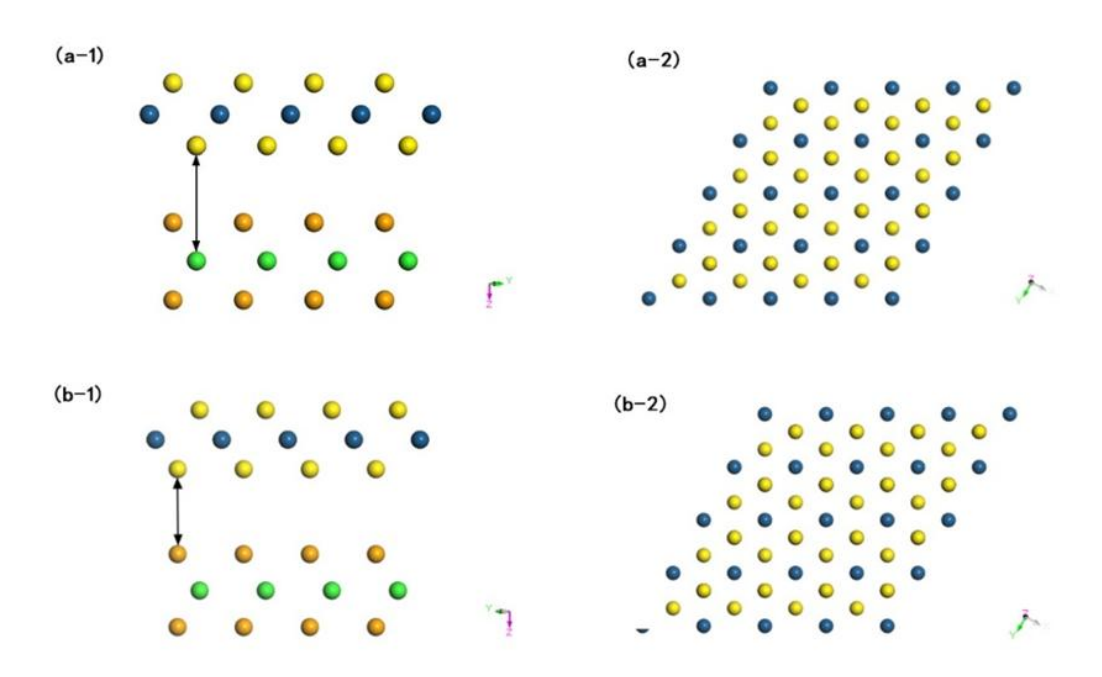


Figure 2. Two combinations of WSe_2 and PtS_2 , Model A (a) and Model B (b). The yellow, orange, green and blue spheres represent S, Se, W and Pt atoms, respectively.

indicating that the values of $U_{\rm Pt}$ and $U_{\rm W}$ are reasonable. As shown in Figure 3(c), the band gap energies of the PtS2/WSe2 heterostructures are 0.775 eV (Model A) and 0.727 eV (Model B), which are significantly reduced compared with the single semiconductor, which will lead to a red shift of the absorption edge. The PDOS data (Figure 4) shows that the valence band of bulk PtS2 is mainly contributed by the p-orbital of S, while the conduction band is dominated by both S p and Pt d. The p-orbital of Se and the d-orbital of W dominate the valence and conduction bands of bulk WSe2, respectively. The similarity of the PDOS of Model A and Model B is that the valence band is mainly contributed by the *d*-orbital of Pt, and the conduction band is mainly contributed by the d-orbital of W. It is can be inferred that, the electrons were excited from the valence band of PtS₂ to the conduction band of WSe₂, which completed the photoexcitation process.

3.3 Electronic Transfer Route

The work function and Mulliken charge population of Model A and Model B were

calculated to study the charge transfer between interfaces in this paper. The work function represents the energy required to move the electrons at the top of the valence band to the vacuum level [32]. As shown in Figure 5, the work functions of PtS₂, WSe₂ and PtS₂/WSe₂ heterostructures are 5.849, 4.869, 4.964 and 5.076 eV, respectively.

The analysis of Mulliken charge is shown in Table 3. There is no charge transfer between layers in Model B, while in Model A, about 0.64 eV of Mulliken charge is transferred from the W layer to the Pt layer. In this paper, it is believed that the electrons and holes of this heterostructure may follow the S-scheme transfer route, and the mechanism is analyzed as follows: When the nanosheets of WSe₂ and PtS₂ are pre-contacted, since the Fermi level of WSe2 is higher than that of PtS₂, electrons will spontaneously transfer from WSe₂ flows to PtS₂, and eventually electrons are depleted at WSe2 and accumulated at PtS2. At this time, a built-in electric field from WSe2 to PtS2 is formed, accelerating the transfer of electrons (holes) to WSe2 conduction band (PtS2 valence

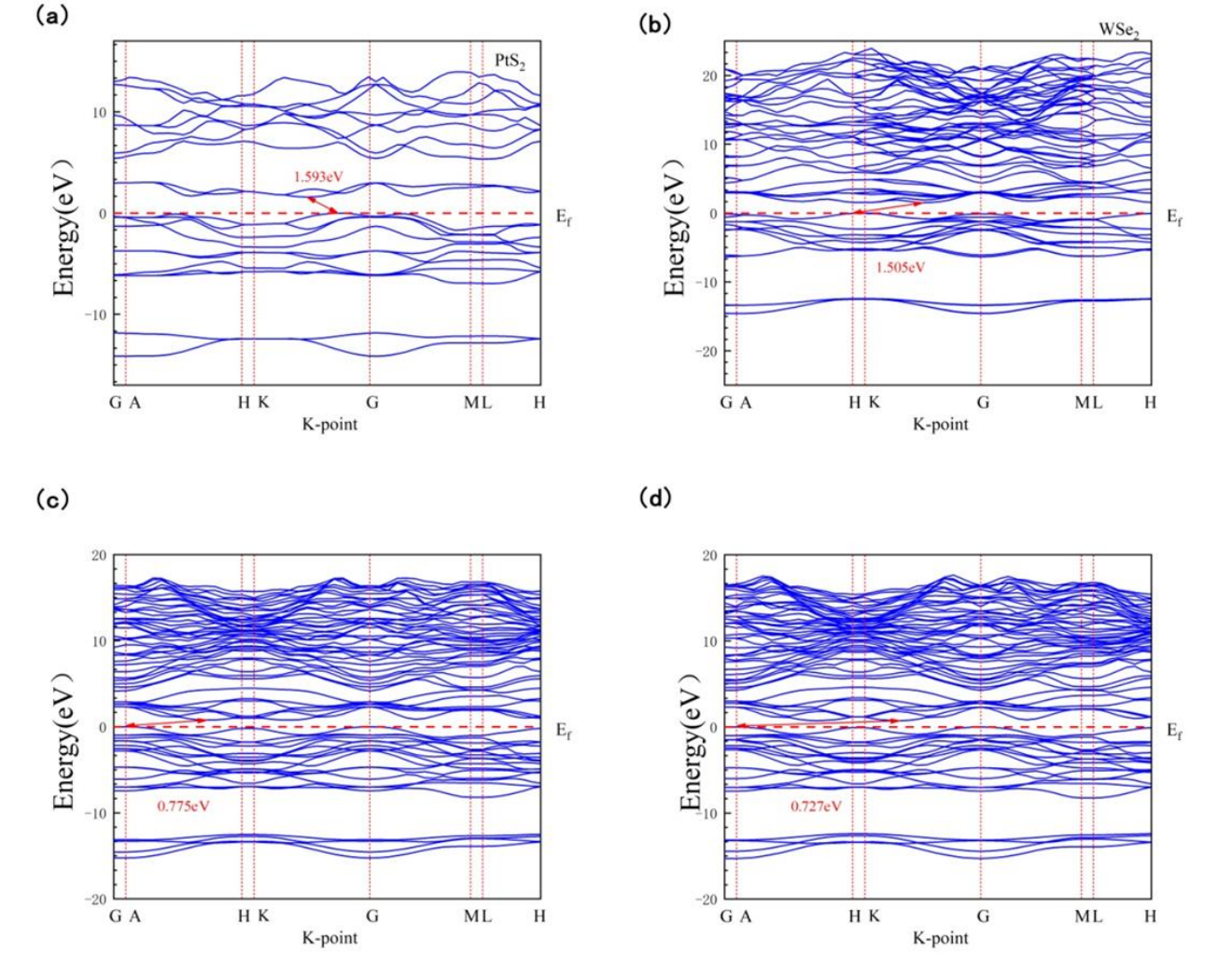


Figure 3. Band structure calculation results of bulk PtS₂ (a), bulk WSe₂ (b), PtS₂/WSe₂ heterostructure Model A (c) and PtS₂/WSe₂ heterostructure Model B (d) The short dashed line with zero ordinate is the Fermi level.

band). The process of Fermi level rearrangement also leads to the band bending of the two semiconductors, that is, the band structure of WSe₂ is bent upward, while that of PtS₂ is bent downward. Driven by band bending, built-in electric field, and Coulomb attraction, the electron-hole pairs with weak redox ability in the

interface region will recombine, while the stronger holes and electrons in VBPtS₂ and CBWSe₂ are preserved.

In order to verify that Model A is an s-scheme heterojunction, we calculated the Electron density difference of Model A. As shown in the Figure 6, red represents the electron accumulation region,

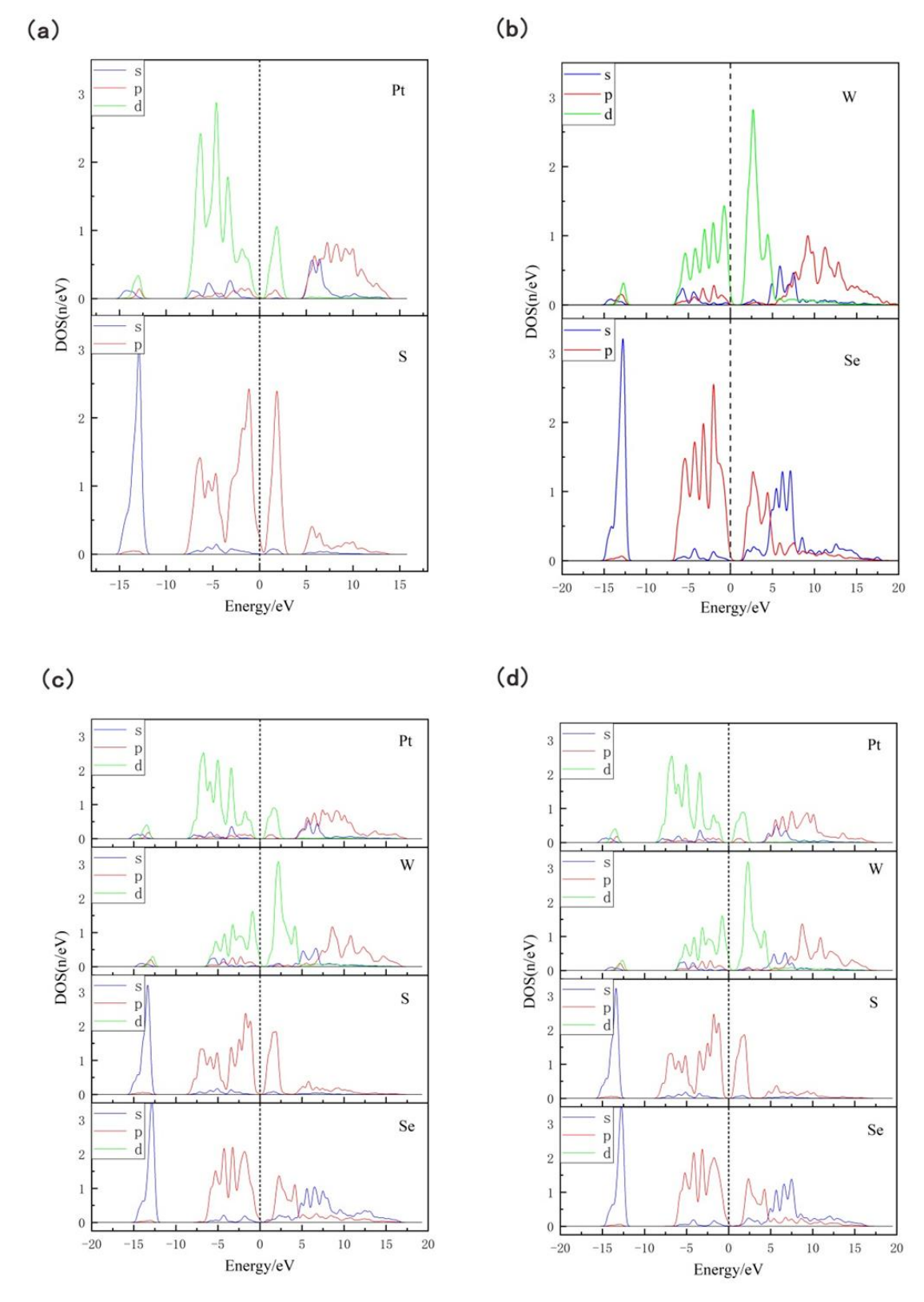


Figure 4. The DOS diagram of bilayer PtS₂ (a), bilayer WSe₂ (b) and PtS₂/WSe₂ heterostructure (c)The short dashed lines represent the Fermi level.

and blue represents the electron depletion region. It can be seen that the electrons are rearranged in the interface region, that is, PtS_2 gains the electrons transferred from WSe_2 , which is due to the Fermi level of PtS_2 being lower than that of WSe_2 , which verifies that the electrons of the Model A heterojunction conform to Inferences for S-scheme transfer routes.

It is worth noting that the data of PDOS also supports our view. As shown in Figure 4, the Fermi level of pristine PtS₂ is located at the top of the valence band. After PtS₂ and WSe₂ are stacked to form a heterojunction, the Fermi level shifts to the right in the fractional density of states of Pt and S, which means that electrons accumulate in the PtS₂ layer.

3.4 Catalytic Ability

The redox potential of water should be spaned by the band edge of the photocatalyst in theory, it

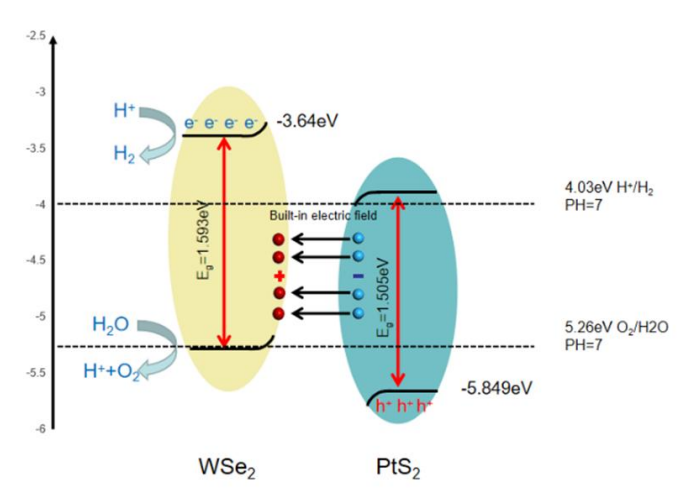


Figure 5. Schematic diagram of PtS₂/WSe₂ heterostructure with band-edge positions.

means that, the CB edge of photocatalysist needs to be more negative than the hydrogen electrode (-4.44 eV, pH = 0), and the VB edge position needs to be more positive than the oxygen electrode (-5.67 eV, pH = 0). The hydroxide electrode potential can be calculated by E = -4.44 (-5.67) eV + pH × 0.059 eV. Since Model A is an S-scheme heterostructure, the weak electrons and holes in the interface region disappear recombination, and $_{
m the}$ electrons in conduction band of PtS2 are transferred to the conduction band of WSe2 under the action of the built-in electric field. The holes in the valence band of WSe2 are transferred to the valence band of PtS2, so the band edge of Model A satisfies the conditions for catalytic water splitting.

3.5 HOMO and LUMO Analyses

Charge separation can be well studied by the highest occupied molecular orbital (HOMO) and the lowest unoccupied molecular orbital (LUMO). The LUMO and HOMO of bilayer PtS₂ and bilayer

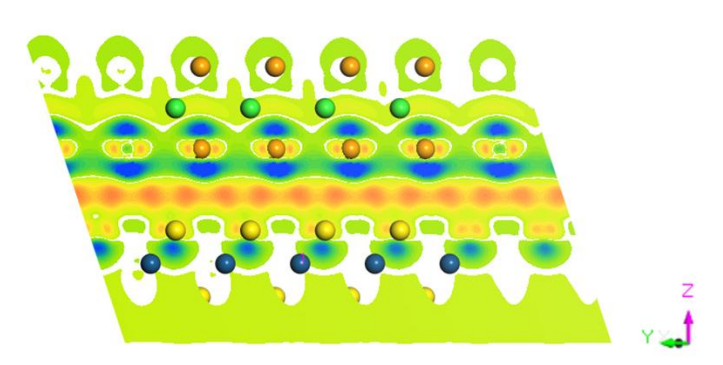


Figure 6. Calculated electron density difference of Model A

Table 3. Mulliken charge populations of bulk PtS₂ (a), bulk WSe₂ (b), PtS₂/WSe₂ heterostructure Model A (c) and PtS₂/WSe₂ heterostructure Model B (d)

Species	Atom	Mulliken charge population						
		s	p	d	f	total	Charge	
PtS_2	S_1	0.94	2.06	0	0	3.00	0.00	
	S_2	0.94	2.06	0	0	3.00	0.00	
	Pt	1.41	3.24	4.35	7.00	16.00	0.01	
WSe_2	S_1	1.70	4.08	10.00	0	15.78	0.22	
	S_2	1.70	4.08	10.00	0	15.78	0.22	
	\mathbf{W}_1	2.68	6.97	4.80	14.00	28.44	-0.44	
PtS ₂ /WSe ₂ (Model A)	S_1	1.87	4.14	0	0	6.01	-0.01	
	S_2	1.86	4.15	0	0	6.01	-0.01	
	Se_1	1.83	4.08	10.00	0	15.91	0.09	
	Se_2	1.70	4.08	10.00	0	15.77	0.23	
	W	2.64	6.84	4.80	14.00	28.28	-0.28	
	Pt	2.84	6.56	8.62	14.00	32.01	-0.01	
PtS ₂ /WSe ₂ (Model B)	S_1	1.87	4.14	0	0	6.01	-0.01	
	S_2	1.87	4.14	0	0	6.00	-0.00	
	Se_1	1.82	4.08	10.00	0	15.91	0.09	
	Se_2	1.75	4.08	10.00	0	15.83	0.17	
	W	2.63	6.83	4.80	14.00	28.26	-0.26	
	Pt	2.84	6.53	8.62	14.00	31.99	0.01	

WSe₂ were shown in Figure 7, which were set as the background to compare the charge separation of Model A and Model B.

We were pleasantly surprised to find that the LUMO-HOMOs of Model A and Model B are almost completely spatially separated compared to bilayer pristine semiconductors (which have almost no separated LUMO-HOMO orbitals). In detail, LUMO is mainly distributed in the W

layer, while HOMO is mainly distributed in the Pt layer. The HOMO and LUMO of the heterojunction catalyst have been completely redistributed, which verifies the existence of the built-in electric field. The spatial separation of LUMO and HOMO suppresses the recombination of photogenerated electrons and holes, greatly enhancing the photocatalytic activity.

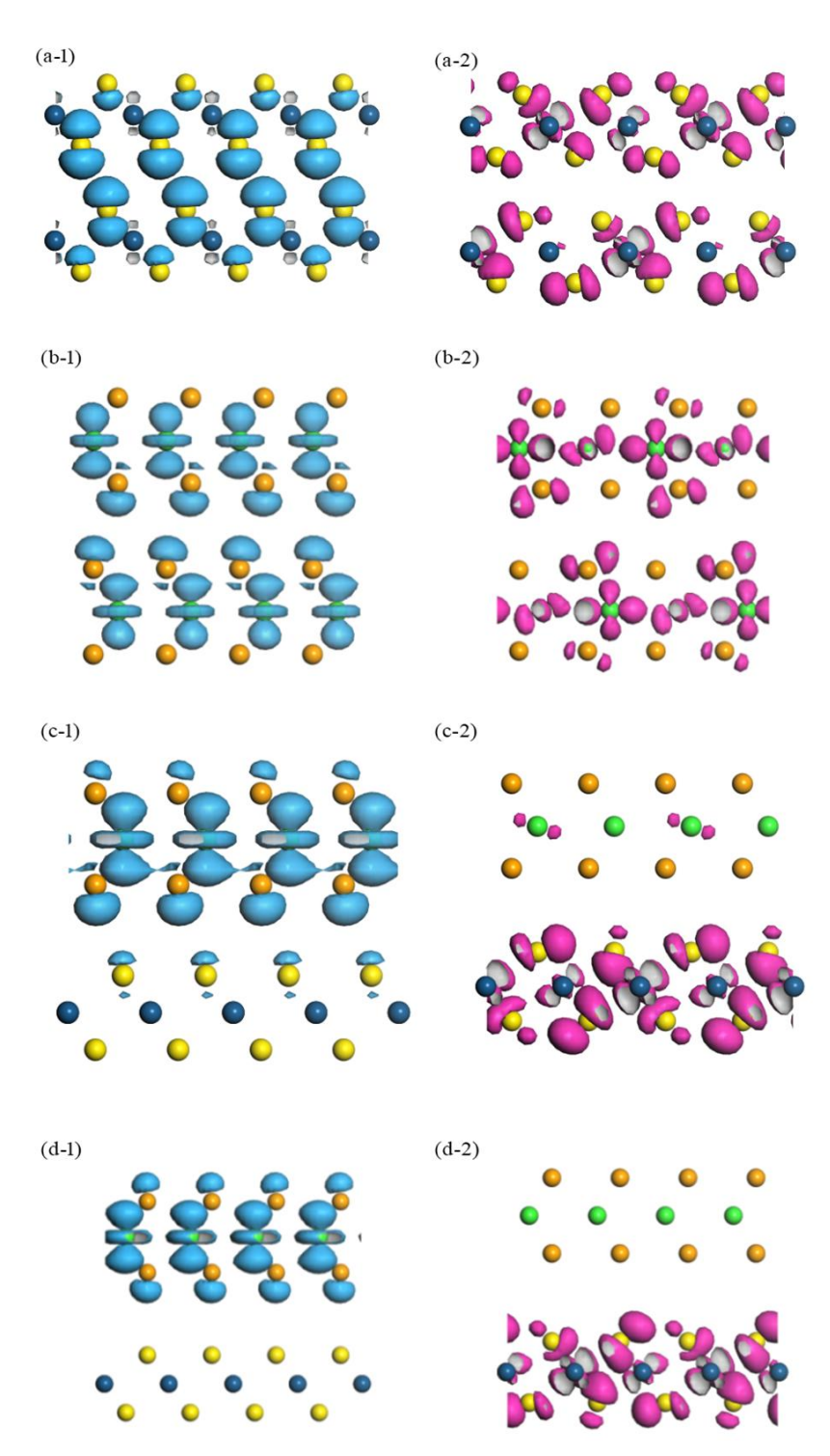


Figure 7. Calculated HOMO of PtS₂ (a-1), WSe₂ (b-1), Model A(c-1) and Model B(d-1). Calculated LUMO of PtS₂ (a-2), WSe₂ (b-2), Model A (c-2) and Model B (d-2). The green, orange, yellow and blue spheres represent W atoms, Se atoms, S atoms and Pt atoms, respectively. The molecular orbitals in purple and in blue are indicating LUMO and HOMO, respectively.

4. Conclusions

In conclusion, we investigated two stacking ways of WSe₂ with PtS₂ by DFT calculations. Based on the definition of adsorption energy, a more stable structure was selected for charge analysis. Mulliken charges and differential charge densities demonstrate that the structure is characteristic of S-scheme catalysts. Due to the height difference between the Fermi levels of pristine WSe₂ and PtS_2 , electrons spontaneously from WSe2 to PtS2, thereby forming a built-in electric field. Under the action of Coulomb gravity, built-in electric field and energy band bending, the weak electrons and holes in the interface region disappear due to recombination, and the strong electrons and holes can be preserved in the conduction band of WSe2 and the valence band of PtS2. The HOMO-LUMO calculations show that the sterically complete separation of HOMO and LUMO suppresses the electron-hole recombination and improves the photocatalytic efficiency. This work finds a new Sheterojunction and theoretically demonstrates its feasibility as a photocatalyst.

Acknowledgements

This work was supported by The Foundation of Liaoning Provincial Key Laboratory of Energy Storage and Utilization (CNWK202302). Special thanks are due to the instrumental analysis from Analytical and Testing Center, Northeastern University.

CRedit Author Statement

Zhaonan Sun: Writing – original draft, Investigation, Validation, Software, analysis, Methodology, Data curation, Funding acquisition. Yuxuan Song: Conceptualization, Formal analysis, Investigation, Methodology, Resources. Wendi Lv: Conceptualization, Resources. Xiangyu Zeng: Writing - review and Investigation, Methodology, editing, Visualization. Zhongtian Fu: Supervision, Project Investigation, Methodology, Administration, Visualization. All authors have read and agreed to the published version of the manuscript.

References

- [1] Bian, X.N., Zhang, S., Zhao, Y.X., Shi, R., Zhang, T.R. (2021). Layered double hydroxide-based photocatalytic materials toward renewable solar fuels production. *Infomat.* 3, 719-738. DOI: 10.1002/inf2.12192.
- [2] Su, Y.Y. (2021). Revisiting carbon, nitrogen, and phosphorus metabolisms in microalgae for wastewater treatment. Science of the Total Environment. 762. DOI: 10.1016/j.scitotenv.2020.144590.

- [3] Wu, Z.Z., Gao, F.Y., Gao, M.R. (2021). Regulating the oxidation state of nanomaterials for electrocatalytic CO₂ reduction. *Energy & Environmental Science*. 14, 1121-1139. DOI: 10.1039/d0ee02747b.
- [4] Subramanyam, P., Meena, B., Biju, V., Misawa, H., Challapalli, S. (2022). Emerging materials for plasmon-assisted photoelectrochemical water splitting. Journal of Photochemistry and Photobiology C-Photochemistry Reviews. 51, 100472. DOI: 10.1016/j.jphotochemrev.2021.100472.
- [5] Acharya, R., Parida, K. (2020). A review on TiO₂/g-C₃N₄ visible-light- responsive photocatalysts for sustainable energy generation and environmental remediation. *Journal of Environmental Chemical Engineering*. 8, 103896. DOI: 10.1016/j.jece.2020.103896.
- [6] Chen, T., Liu, L.Z., Hu, C., Huang, H.W. (2021). Recent advances on Bi₂WO₆-based photocatalysts for environmental and energy applications. *Chinese Journal of Catalysis*. 42, 1413-1438. DOI: 10.1016/S1872-2067(20)63769-X.
- [7] Chen, S., Liu, T.X., Zheng, Z.H., Ishaq, M., Liang, G.X., Fan, P., Chen, T., Tang, J. (2022). Recent progress and perspectives on Sb₂Se₃-based photocathodes for solar hydrogen production via photoelectrochemical water splitting. *Journal of Energy Chemistry*. 67, 508-523. DOI: 10.1016/j.jechem.2021.08.062.
- [8] Shandilya, P., Sambyal, S., Sharma, R., Mandyal, P., Fang, B.Z. (2022). Properties, optimized morphologies, and advanced strategies for photocatalytic applications of WO₃ based photocatalysts. *Journal of Hazardous Materials*. 428. DOI: 10.1016/j.jhazmat.2022.128218.
- [9] Astuti, Y., Musthafa, F., Arnelli, A., Nurhasanah I. (2022). French Fries-Like Bismuth Oxide: Physicochemical Properties, Electrical Conductivity and Photocatalytic Activity. Bulletin of Chemical Reaction Engineering & Catalysis. 17(1), 146-156. DOI: 10.9767/bcrec.17.1.12554.146-156.
- [10] Astuti, Y., Mulyana, T.N., Tasiman, B.H.A., Darmawan, A., Widyandari, H. (2023). Hydrazine-Fueled Solution Combustion Method: Fuel/Oxidizer Ratio Effects on Photocatalytic Performance of Bismuth Oxide. Bulletin of Chemical Reaction Engineering & Catalysis. 18(3), 539-547. DOI: 10.9767/bcrec.19943.
- [11] Opoku, F., Govender, K.K., van Sittert, C.G.C. E., Govender, P.P. (2018). Understanding the synergistic effects, optical and electronic properties of ternary Fe/C/S-doped TiO₂ anatase within the DFT plus U approach. *International Journal of Quantum Chemistry*. 118(5). DOI: 10.1002/qua.25505.

- [12] Acharya, L., Nayak, S., Pattnaik, S.P., Acharya, R., Parida, K. (2020). Resurrection of boron nitride in p-n type-II boron nitride/B-doped-g-C₃N₄ nanocomposite during solid-state Z-scheme charge transfer path for the degradation of tetracycline hydrochloride. *Journal of Colloid and Interface Science* .566, 211-223. DOI: 10.1016/j.jcis.2020.01.074.
- [13] Acharya, R., Parida, K. (2020). A review on TiO₂/g-C₃N₄ visible-light- responsive photocatalysts for sustainable energy generation and environmental remediation. *Journal of Environmental Chemical Engineering*, 8. DOI: 10.1016/j.jece.2020.103896
- [14] Fu, J.W., Xu, Q.L., Low, J.X., Jiang, C.J., Yu, J.G. (2019).Ultrathin 2D/2D WO3/g-C3N4 step-scheme H2-production photocatalyst. *Applied Catalysis B: Environmental.* 243, 556-565. DOI: 10.1016/j.apcatb.2018.11.011
- [15] Xu, Q., Zhang, L., Cheng, B., Fan, J., Yu J. (2020). S-Scheme Heterojunction Photocatalyst. *Chem.* 6, 1543-1559. DOI: 10.1016/j.chempr.2020.06.010.
- [16] Liu, B., Bie, C., Zhang, Y., Wang, L., Li, Y., Yu, J. (2021). Hierarchically Porous ZnO/g-C₃N₄ S-Scheme Heterojunction Photocatalyst for Efficient H₂O₂ Production. Langmuir. 37, 14114-14124. DOI: 10.1021/acs.langmuir.1c02360.
- [17] Pham, V.V., Mai, D.Q., Bui, D.P., Man, T.V., Cao, T.M. (2021). Emerging 2D/0D g-C₃N₄/SnO₂ S-scheme photocatalyst: New generation architectural structure of heterojunctions toward visible-light-driven NO degradation. *Environmental Pollution*. 286, 117510. DOI: 10.1016/j.envpol.2021.117510.
- [18] Jiang, Y, Sun, Z., Chen, Q., Cao, C., Zhao, Y., Yang, W., Zeng, L., Huang, L. (2022). Fabrication of 0D/2D TiO₂ Nanodots/g-C₃N₄ S-scheme heterojunction photocatalyst for efficient photocatalytic overall water splitting. Applied Surface Science. 571, 151287. DOI: 10.1016/j.apsusc.2021.151287.
- Zhang, L., Zhang, J., Yu, H., Yu, J. (2022).
 Emerging S-Scheme Photocatalyst. Advanced Materials. 34, 2107668. DOI: 10.1002/adma.202107668.
- [20] Fiori, G., Bonaccorso, F., Iannaccone, G., Palacios, T., Neumaier, D., Seabaugh, A., Banerjee, S.K., Colombo, L. (2014). Electronics based on two-dimensional materials. *Nature Nanotechnology*. 9, 768-779. DOI: 10.1038/nnano.2014.207.
- [21] Pumera, M., Sofer, Z., Ambrosi, A. (2014). Layered transition metal dichalcogenides for electrochemical energy generation and storage. *Journal of Materials Chemistry A.* 2, 8981-8987. DOI: 10.1039/c4ta00652f.
- [22] Li, L., Long, R., Prezhdo, O.V. (2017). Charge Separation and Recombination in Two-Dimensional MoS₂/WS₂: Time-Domain ab Initio Modeling .*Chemistry of Materials*. 29, 24662473. DOI: 10.1021/acs.chemmater.6b03727.

- [23] Jariwala, D., Sangwan, V.K., Lauhon, L.J., Marks, T.J., Hersam, M.C. (2014). Emerging Device Applications for Semiconducting Two-Dimensional Transition Metal Dichalcogenides. ACS Nano. 8, 1102-1120. DOI: 10.1021/nn500064s.
- [24] Britnell, L., Ribeiro, R.M., Eckmann, A., Jalil, R., Belle, B.D., Mishchenko, A., Kim, Y.J., Gorbachev, R.V., Georgiou, T., Morozov, S.V., Grigorenko A.N., Geim A.K., Casiraghi C., Castro Neto A.H. and Novoselov K.S .(2013). Strong Light-Matter Interactions in Heterostructures of Atomically Thin Films. Science. 340, 1311-1314. DOI: 10.1126/science.1235547.
- [25] Zhu, L., Ding, Y., Yang, W., Yin, S., Cai M. (2021). Effects of doping on photocatalytic water splitting activities of PtS2/SnS2 van der Waals heterostructures. *Physical Chemistry Chemical Physics*. 23, 18125. DOI: 10.1039/d1cp01777b.
- [26] Morgan, W.S., Christensen, J.E., Hamilton, P.K., Jorgensen, J.J., Campbell, B.J., Hart, G.L.W., Forcade, R.W. (2020). Generalized regular kpoint grid generation on the fly. *Computational Materials Science*. 173, 109340. DOI: 10.1016/j.commatsci.2019.109340.
- [27] Hardcastle, T.P., Seabourne, C.R., Zan, R., Brydson, R.M.D., Bangert, U., Ramasse, Q.M., Novoselov, K.S., Scott, A.J. Mobile metal adatoms on single layer, bilayer, and trilayer graphene: An ab initio DFT study with van der Waals corrections correlated with electron microscopy data. *Physical Review B*. 87, 195430. DOI: 10.1103/PhysRevB.87.195430.
- [28] Wei, X.B., Yang, L., Sun, S.H., Zhao, Y.S., Liu, H.D. (2024). Strain-induced effects on the optoelectronic properties of ZrSe₂/HfSe₂ heterostructures. *Journal of Molecular Modeling*. 30, 3. DOI: 10.1007/s00894-023-05793-0.
- [29] Almayyali, A.O.M., Kadhim, B.B., Jappor, H.R. (2020). Stacking impact on the optical and electronic properties of two-dimensional MoSe₂/PtS₂ heterostructures formed by PtS₂ and MoSe₂ monolayers. *Chemical Physice*. 532, 110679. DOI: 10.1016/j.chemphys.2020.110679.
- [30] Sun, M., Chou, J., Yu, J., Tang, W. (2017). Effects of structural imperfection on the electronic properties of graphene/WSe₂ heterostructures. *Journal of Materials Chemistry C.* 5, 10383. DOI: 10.1039/c7tc03131a.
- [31] Aikens, C.M. (2018). Electronic and Geometric Structure, Optical Properties, and Excited State Behavior in Atomically Precise Thiolate-Stabilized Noble Metal Nanoclusters. *Accounts of Chemical Research*. 51, 21, 3065-3073. DOI: 10.1021/acs.accounts.8b00364.
- [32] Li, X.B., Liu, J.Y., Huang, J.T., He, C.Z., Feng, Z.J., Chen, Z., Wan, L.Y., Deng, F. (2021). All Organic S-Scheme Heterojunction PDI-Ala/S-C3N4 Photocatalyst with Enhanced Photocatalytic Performance. Acta Physico-Chimica Sinica. 37, 6. DOI: 10.3866/pku.whxb202010030.